Finite Element Solutions for Magnetic Shielding Power Applications

Dumitru Cazacu, Elena Otilia Virjoghe, Valeriu Manuel Ionescu, and Stefan Castravete

Abstract In this chapter are presented some aspects concerning the finite element analysis of magnetic shielding for power applications. The investigation describes the physical mechanisms of magnetic shielding the magnetic field in a cylindrical shield using magnetic scalar potential and magnetic vector potential. A variational and a Galerkin finite element formulation are described. The mitigation of an OHTL magnetic field inside a shielded building placed near it is evaluated in the case study of this chapter.

Keywords Low frequency magnetic field · Power application · Finite element · Passive magnetic shielding

Symbols and Acronyms

OHTL	Overhead transmission lines
UGTC	Underground transmission cables
MV/LV	Medium voltage/low voltage
CAE	Computer aided engineering
FEM	Finite Element Method
SE	Shielding effectiveness

D. Cazacu (✉) · V. M. Ionescu
University of Pitesti, Pitesti, Romania
e-mail: dumitru.cazacu@upit.ro

V. M. Ionescu
e-mail: valeriu.ionescu@upit.ro

E. O. Virjoghe
University Valahia, Targoviste, Romania
e-mail: elena.virjoghe@valahia.ro

S. Castravete
CAELYNX-Europe, Craiova, Romania
e-mail: scastravete@caelynx.ro

N. Mahdavi Tabatabaei and N. Bizon (eds.), *Numerical Methods for Energy Applications*, Power Systems,
https://doi.org/10.1007/978-3-030-62191-9_27

MSP V_m	Magnetic scalar potential V_m
MVP A	Magnetic potential vector A
δ	Skin depth
$\omega = 2\pi f$	Angular frequency
μ_0	Vacuum magnetic absolute permeability
μ_r	Relative magnetic permeability
σ	Electric conductivity
H	Magnetic field strength
E	Electric field strength
k	Propagation constant
B	Magnetic flux density
J	Current density
SLF	Super low frequency
PDE	Partial Differential Equation
Ni	Shape functions

1 Introduction

The electromagnetic pollution progressed a lot in the last century. The diversity of the electric and electronic systems has evolved in a tremendous way. Those devices operate in different frequency ranges, concentrated on specialized spectral domains.

Some of the most common sources of low frequency magnetic fields are the overhead transmission lines (OHTL), underground transmission cables (UGTC), medium voltage/low voltage (MV/LV) substations and building's electrical distribution systems. Their magnetic fields can generate electromagnetic compatibility problems caused the interference that affects technical features of the electrical and electronic devices and also can represent potential hazards for the human health.

In order to evaluate the possibilities of mitigating the magnetic field of these equipments and to compare the results with the reference values proposed by the international scientific institutions some methods were proposed.

In [1] certain intrinsic and extrinsic methods are described. The first category is referring to modifying the geometrical and electrical parameters of the magnetic field source: layout and compaction, distance management, phase splitting and phase cancellation. The second one comprises passive and active techniques depending on the way in which they attenuate the magnetic field.

The passive solutions refer to the attenuation systems that are located near the source of the magnetic field or in the neighborhood of the protected region.

Passive solutions include conductive and/or ferromagnetic shields and passive loops.

Active solutions use external devices that generates magnetic field that attenuate the incident magnetic field, having the same magnitude, phase and frequency. They are used in so called active loops. These are complex and expensive devices that

monitors and adjust the necessary current in order to obtain the proper counterpart magnetic field [2].

In order to design and evaluate the effectiveness of the attenuation solution generally computer aided engineering (CAE) software tools are used [3, 4].

Analytical solutions exist only for simple geometries and homogenous media.

Those programs use different numerical techniques in order to solve the specific forms of Maxwell equations that describe the operating of the considered systems. The most used methods are the finite difference method, the finite element method, the boundary element method and the transmission line matrix method.

One of the most versatile numerical methods used to simulate electromagnetic fields is the finite element method.

Modeling and simulation of the magnetic shields for power applications by the finite element method is widely described in the literature.

In [5] a precise shielding factor computation, based on the Finite Element Method (FEM) combined with the Jiles-Atherton model is presented, considering random disturbances. In paper [6] the 3D magnetic field of the reactor is computed by the method of edge-node finite element coupling.

In [7, 8] some numerical problems for magnetostatic and time harmonic 3D magnetic shields are presented in [9] different types of magnetic potentials are used for computing 3D magnetostatic shields effectiveness.

The effectiveness of the multilayer magneto static and time harmonic shields is evaluated using finite element method in [10, 11].

In [12] one and two shells magneto static cylindrical shields were considered. Applying the interface conditions at the discontinuity surfaces between the media, the symbolic algebraic systems of equations for those configurations were obtained and solved. Structure of the system's matrices were analyzed and their sparsity patterns were visualized. Analytical and numerical transversal effectiveness of the cylindrical shields were computed for different lengths.

Some numerical and experimental aspects concerning the electromagnetic shielding in microwave range are presented in [13, 14].

Measured values of the electrical field for an open type air substation are compared with numerical results obtained by finite element program Ansys in [15].

One of the new trends in computational electromagnetics is using the multicore machines in order to improve the execution time. Aspects concerning this topic applied for Comsol Multiphysics on a 3D magnetostatic problem are available in [16–17].

In [18] analytic and numerical comparison between the magnetic stored energy in cylindrical and toroidal coils considering the steady state superconducting state is considered.

Numerical shielding solutions concerning the underground power cables, using FEMM finite element software, are described in [19, 20]. In [21] a combination of theoretical analysis and numerical simulations with the finite element method is used to analyze the shielding properties of a passive and active shield developed for a SERF co-magnetometer application.

The progresses in the development of CAE programs that use finite element method are presented in many scientific papers.

In [22] certain recent trends in computational electromagnetics for defense applications are presented. Numerical aspects referring to an a posteriori error estimate of weak Galerkin (WG) finite element methods that can be applied to polygonal meshes and to an ill-posed elliptic Cauchy problems are described in [23, 24].

In this chapter recent trends of using finite element method for the modeling and simulation of passive shielding for low frequency field considering power applications are described.

The structure of the chapter is as follows.

In Sect. 1 is the introduction. Section 2 is entitled Time harmonic magnetic shields. It has two sub sections: Basics magnetic shielding mechanisms and the factors that determine the shielding effectiveness (SE) are described in Sect. 2.1. Solutions of the transversal time harmonic magnetic field in cylindrical shields are obtained in Sects. 2.2.1 and 2.2.2 using the magnetic scalar potential (MSP) and the magnetic potential vector (MVP), respectively. In both cases the shielding effectiveness (SE) was computed and analyzed.

The finite element method is described in Sect. 3, using two formulations.

A variational approach is presented for the magneto static field in Sect. 3.1 and the Galerkin approach is used for the time harmonic magnetic field in Sect. 3.2.

In Sect. 4 a case study that evaluates de magnetic protection of a partially shielded building to the magnetic field produced by an OHTL is presented, using the Ansys finite element software.

The distribution of the magnetic shield inside the building, with and without the shield is described and the maximum values are compared with the reference values indicated by the international commissions.

2 Time Harmonic Magnetic Shields

2.1 Basics of Magnetic Shielding Mechanisms

This type of shields is used to protect some volumes against time variable magnetic fields.

There are shields with closed and open geometries. The first type includes those shields that separate completely the source field and the protected region: the infinite extended plane, the infinite extended cylindrical and the spherical shields [2, 25–26]. For this type the magnetic field occurs in the shielded region by penetration.

For opened geometries (finite length plane shields and finite length cylindrical shields) out of the penetration mechanism appears also the flux leakage.

Two different mechanisms are present in the shielding of low frequency magnetic fields: magnetic flux shunting and magnetic flux attenuation by eddy currents.

The first mechanism is used also for dc magnetic fields [27].

The magnetic flux flows mainly through high permeability magnetic materials, that attract and shunt the flux lines. As a consequence, the magnetic flux lines are concentrated in the shield and avoid the protected region. The shield behaves like a magnetic field concentrator. The shielding effectiveness (SE) depends on the material magnetic permeability, on the geometry (ratio of the thickness over the external diameter multiplied with the magnetic relative permeability), on the shape of the shield and on the thickness of it [25–26, 28, 29].

In the second case the shielding effect is based on the generation of eddy currents in the metallic shells of the enclosure. Eddy currents are induced only in electrically conducting materials. The eddy currents create magnetic fluxes that oppose to the variation of the incident magnetic fluxes. As a consequence, the incident magnetic field is rejected in the neighborhood of the shield [25, 30, 29]. This phenomenon is encountered only in ac magnetic field.

The mechanism is valid no matter what is the value of the magnetic permeability.

Anyway, for materials that have high magnetic permeability the shielding is very efficient. The level of shielding depends on the material permeability and conductivity, on the geometry (ratio of the thickness over the external diameter multiplied with the magnetic relative permeability), on the thickness of the shield and on the frequency of the field source [27].

The eddy current density depends on the frequency of the incident field and on the electric conductivity of the material.

In Fig. 1 the distribution of the magnetic field lines is compared considering two types of magnetic shields: a magneto static cylindrical ferromagnetic shield and a time harmonic magnetic cylindrical shield. The thickness of the shield is 3 mm and the external diameter is 56 mm. The relative magnetic permeability is $\mu_r = 1000$ the electric conductivity $\sigma\ \sigma = 1.45 \cdot 10^6$ S/m and is 50 Hz.

For electromagnetic shields there is an important parameter, called skin depth, which influences the effectiveness of the shield. The expression of it is:

$$\delta = \sqrt{\frac{2}{\omega \mu_0 \mu_r \sigma}} \tag{1}$$

where ω is the angular frequency, μ_r and μ_0 are the relative and absolute magnetic permeability respectively and σ is the electric conductivity of the shield material.

The magnetic field decays in the shield over a distance of few skin depth lengths.

For the shield effectiveness is important the ratio between the thickness and the skin depth g/δ.

If $g \neq \delta$ high values of shield effectiveness could be obtained. If $g = \delta$ the eddy currents have a uniform distribution in the shield thickness and the effectiveness of the shield is less than in the previous case.

For the shields that attenuate the incident field by the mechanism of the eddy current a good effectiveness can be obtained by increasing the maximum dimension, such as the diameter, for a constant thickness.

For the flux shunting mechanism, the increasing of the diameter decreases the SE.

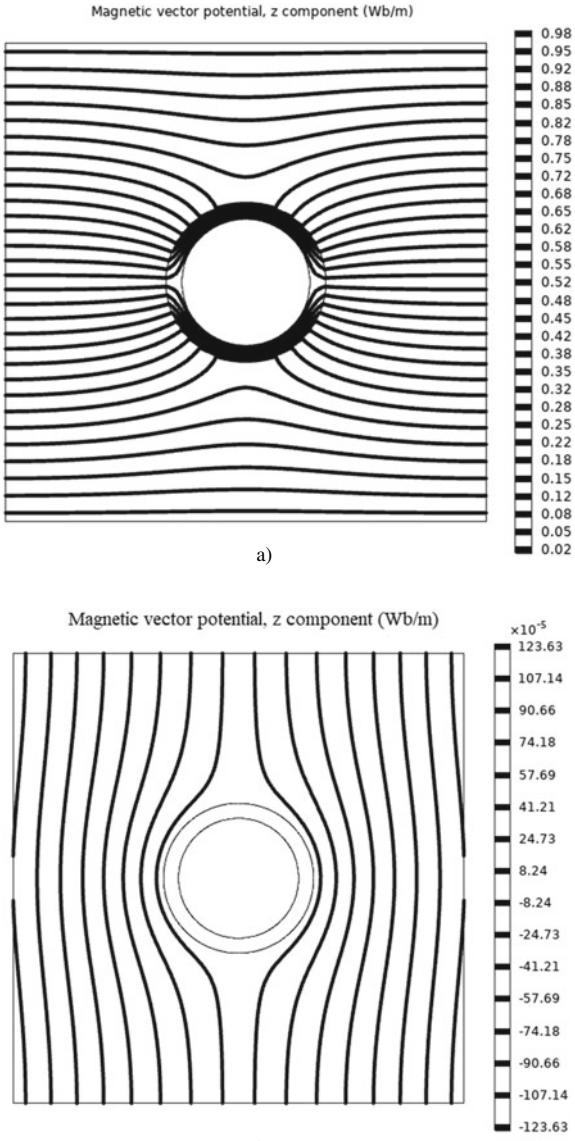

Fig. 1 **a** Magneto static shield as a magnetic field concentrator. **b** Rejection of the magnetic flux lines

In order to increase the SE of the magnetic shields at low frequencies materials with high permeability should be used. But they are expensive and heavy. Mu-Metal and Permalloy are examples of alloys with permeability of up to 100,000, by comparison with ordinary steel that has only few thousands.

A solution to avoid the drawbacks of using those materials is to use a multilayer geometry, composed of combination of ferromagnetic and non ferromagnetic

materials separated by a layer of air. The thickness of the air influences directly the shield effectiveness. Also, two layer shields composed of steel-copper are very efficient against variable magnetic fields. The copper, having high electric conductivity, generates high reflexivity and eddy currents. The steel having high magnetic permeability is proper for low frequencies [21, 31, 32].

One of the new trends for shielding materials is the usage of materials with nonconventional electromagnetic properties, e.g. epsilon-, mu- and index-near-zero metamaterials. They are artificial materials with properties that are not found in nature, e.g. negative permeability. Those materials are manufactured from repetitive structures composed of composite materials such as metals and plastics. In [32] a longitudinal mu-near-zero metamaterial is used to shield quasi-stationary magnetic fields.

2.2 The Cylindrical Shield in Transversal Time Harmonic Magnetic Field

Solutions of the magnetic field equations in the cylindrical shield structure can be obtained using magnetic scalar potential (MSP) or magnetic vector potential(MVP). Both approaches will be presented in the next paragraphs.

2.2.1 Solution Using Magnetic Scalar Potential

The cylindrical and planar shields are mainly used to attenuate the SLF (super low frequency) magnetic field.

In this section a cylindrical shield subjected to a transversal time harmonic magnetic field is analyzed.

In Fig. 2 the cylindrical shield has an external diameter $2r_e$, an inner diameter $2r_i$ and the thickness of the shell is $g = r_{ext} - r_{\text{int}}$. The incident transversal magnetic field is $\overline{H_{ext}} = H_{ext}\overline{j}$, oriented in the Oy direction. The shield is considered to be very long and the end effects are neglected.

From the magnetic point of view there are three domains of interest: outside the shield (region 1), inside the shield wall (region 2) and in the interior of the shield (region 3).

(a) **The electromagnetic field equations in domain 1** $r > r_e$

In this domain there are no current densities. The magnetic field strength can be expressed using the MSP [25–26, 33–34]:

$$rot\underline{\overline{H}} = 0 \tag{2}$$

$$\underline{\overline{H}} = -grad\, V_m \tag{3}$$

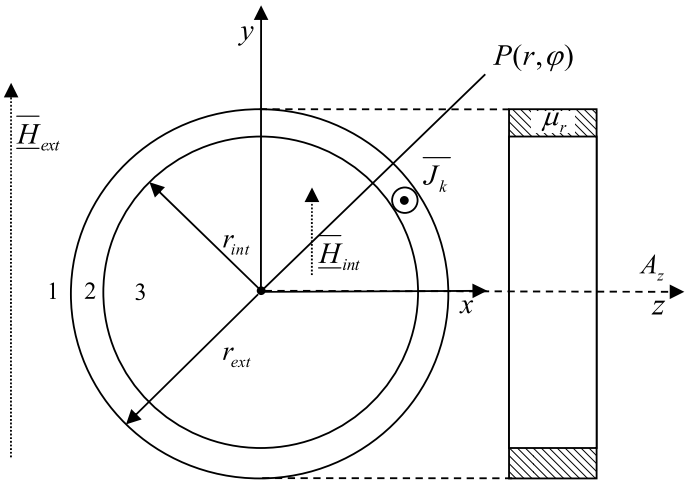

Fig. 2 Cylindrical shield subjected to a transverse time harmonic magnetic field

where V_m is the magnetic scalar potential.

Because $div\ \underline{H} = 0$ it follows that:

$$div\ (\text{grad}\ V_m) = \Delta V_m = 0 \tag{4}$$

In cylindrical coordinates, neglecting the end effects, expression (4) becomes:

$$\Delta V_m = \frac{\partial^2 V_m}{\partial r^2} + \frac{1}{r} \cdot \frac{\partial V_m}{\partial r} + \frac{1}{r^2} \cdot \frac{\partial^2 V_m}{\partial \varphi^2} = 0 \tag{5}$$

In order to solve Eq. 5 the method of separation of variables is used [30, 33–34]:

$$V_m(r, \varphi) = R(r) \cdot \phi(\varphi) \tag{6}$$

The solutions obtained for R and ϕ are:

$$R(r) = C_1 \cdot r^m + C_2 \cdot r^{-m} \tag{7}$$

$$\phi(\varphi) = B_1 \cdot \cos(m\varphi) + B_2 \cdot \sin(m\varphi) \tag{8}$$

and the general expression of the magnetic scalar potential is:

$$V_m(r, \varphi) = \sum_{m=1}^{\infty} \left(C_1 \cdot r^m + C_2 \cdot r^{-m}\right)(B_1 \cos(m\varphi) + B_2 \sin(m\varphi)) \tag{9}$$

After considering the behaviour of the magnetic field far away from the shield, the MSP expression (8) in the domain 1 becomes:

$$V_{m1} = -\left(\underline{H}_{ext} r + C_2 r^{-1}\right) \sin\varphi \tag{10}$$

The magnetic field strength H has the following components:

$$\underline{H_r} = -\frac{\partial V_m}{\partial r} = \left(\underline{H}_{ext} - \frac{C_2}{r^2}\right) \sin\varphi \tag{11}$$

$$\underline{H_\varphi} = -\frac{1}{r} \cdot \frac{\partial V_m}{\partial \varphi} = \left(\underline{H}_e + \frac{C_2}{r^2}\right) \cos\varphi \tag{12}$$

(b) **The electromagnetic field equations in domain 2** $r_{\text{int}} < r < r_{ext}$

In this domain with electrical conductivity the electromagnetic Helmholtz equationdescribes the field [30, 26, 33–35]:

$$\Delta\underline{E} - k^2\underline{E} = 0;\ k^2 = j\omega\mu\sigma \tag{13}$$

where k is the propagation constant for metals.

Because the electric field and the current density are oriented in the 0 z direction we rewrite Eq. 13 in cylindrical coordinates, without vectorial notations:

$$\frac{\partial^2 \underline{E}}{\partial r^2} + \frac{1}{r}\frac{\partial \underline{E}}{\partial r} + \frac{1}{r}\frac{\partial^2 \underline{E}}{\partial \varphi^2} = k^2 \underline{E} \tag{14}$$

Using the separation of the variables the following equations are obtained:

$$\frac{d^2 \underline{E}}{dr^2} + \frac{1}{r}\frac{d\underline{E}}{dr} - \left(k^2 + \frac{n^2}{r^2}\right)\underline{E} = 0 \tag{15}$$

$$\frac{d^2 \underline{E}}{d\varphi^2} + n^2 \underline{E} = 0 \tag{16}$$

Their solutions are:

$$\underline{E}(r) = D_1 I_n(kr) + D_2 K_n(kr) \tag{17}$$

$$\underline{E}(\varphi) = D_3 \cos(n\varphi) + D_4 \sin(n\varphi) \tag{18}$$

We obtain the general solution of (13) as follows:

$$\underline{E}(r, \varphi) = \sum_{n=1}^{\infty} (D_1 I_n(kr) + D_2 K_n(kr))(D_3 \cos(n\varphi) + D_4 \sin(n\varphi)) \tag{19}$$

This solution comprises the modified Bessel functions, of order n, $I_n(kr)$ and $K_n(kr)$.

This solution is proper when the thickness of the shield $g = r_2 - r_1$ is significant by comparation with the radius r_{ext}.

For practical shields, the thickness verifies $g << r_i$.

If the condition $n^2/r^2 << |k^2|$ is fulfilled, then Eq. 15 becomes [30]:

$$\frac{d^2\underline{E}}{dr^2} + \frac{1}{r}\frac{d\underline{E}}{dr} - k^2\underline{E} = 0 \tag{20}$$

and have the solution:

$$\underline{E}(r) = M_1 e^{kr} + M_2 e^{-kr};\ k = \sqrt{j\omega\mu\sigma} \tag{21}$$

The solution of electric field in the shield wall is:

$$\underline{E}(r, \varphi) = \left(M_1 e^{kr} + M_2 e^{-kr}\right)\cos\varphi \tag{22}$$

(c) **The electromagnetic field equations in domain 3**

In this domain the magnetic field is described by similar equations similar with (11) and (12) but without the terms C_2/r^2, because when $r \to 0$ the magnetic field goes to infinite [30, 26, 35, 36].

The expressions of the magnetic field components are:

$$\underline{H}_r = \underline{H}_{ext}\sin\varphi \tag{23}$$

$$\underline{H}_\varphi = \underline{H}_{ext}\cos\varphi \tag{24}$$

The shielding factor

In order to compute the shielding factor the interface conditions among those three domains are used. The shielding factor $\underline{SF}$ is a complex number and is defined by the ratio:

$$\underline{SF} = \underline{H_{\text{int}}}/\underline{H_{ext}} \tag{25}$$

Interface conditions

At the border between the first and the second domains, for $r = r_{ext}$, the normal component of the magnetic flux density and the tangential component of the magnetic field strength are preserved.

As a consequence the following expressions are obtained:

$$\underline{H}_{ext} - \frac{C_2}{r_{ext}^2} = \frac{1}{j\omega\mu_0 r_m}\left(M_1 e^{kr_{ext}} + M_2 e^{-kr_{ext}}\right) \tag{26}$$

$$\underline{H}_{ext} + \frac{C_2}{r_{ext}^2} = \frac{k}{j\omega\mu}\left(M_1 e^{k_{ext} r} - M_2 e^{-k r_{ext}}\right) \tag{27}$$

At the boundary between the second and the third domain, for $r = r_{\text{int}}$, from the same conditions the next expressions follows:

$$\underline{H}_{\text{int}} = \frac{1}{j\omega\mu_0 r_m}\left(M_1 e^{k r_{\text{int}}} + M_2 e^{-k r_{\text{int}}}\right) \tag{28}$$

$$\underline{H}_{\text{int}} = \frac{k}{j\omega\mu}\left(M_1 e^{k r_{\text{int}}} - M_2 e^{-k r_{\text{int}}}\right) \tag{29}$$

From relations (26) to (29) the following unknowns C_2, M_1, M_2, H_{int} are obtained. After the calculation, the expression of the shielding factor is obtained:

$$\underline{F}_e = \frac{\underline{H}_{\text{int}}}{\underline{H}_{ext}} = \frac{1}{\cosh kg + \frac{1}{2}\left(D + \frac{1}{D}\right)\sinh kg} \tag{30}$$

where k is the propagation constant in metals:

$$\underline{k} = \sqrt{j\omega\sigma\mu} = \frac{1+j}{\delta} \tag{31}$$

and D is:

$$D = \frac{k r_m}{\mu_r} \tag{32}$$

and $g = r_e - r_i$ is the thickness of the shield.

Because $g << r_i$ the following approximation have been used: $r_e \approx r_i = r_m$ The SE can be computed using the following expression:

$$SE = \left|\frac{1}{\underline{SF}}\right| = \sqrt{\text{Re}^2\left(1/\underline{F_e}\right) + \text{Im}^2\left(1/\underline{F_e}\right)} \tag{33}$$

The shield effectiveness SE increases with the thickness of the shield wall and with the frequency of the incident field. Ferromagnetic cylindrical shields have higher SE values, at the same thickness, magnetic permeability and frequency than those manufactured from non ferromagnetic materials.

2.2.2 Solution Using Magnetic Potential Vector

The same problem can be solved in terms of the magnetic vector potential A in a cylindrical reference coordinate system. The geometry is symmetrical and the

magnetic vector potential is oriented in the z direction and it is independent of the z coordinate. In domains 1 and 3 of the cylindrical shield, the magnetic vector potential verifies the Laplace equation and in domain 3 the shield verifies the diffusion equation [2, 30, 34]:

$$\nabla^2 A_z = 0, r \geq r_{ext} \tag{34}$$

$$\nabla^2 A_z - k^2 A_z = 0, r_{\text{int}} < r < r_{ext} \tag{35}$$

$$\nabla^2 A_z = 0, r \leq r_{\text{int}} \tag{36}$$

where

$$\nabla^2 A_z = (\frac{\partial^2}{\partial r^2} + \frac{1}{r}\frac{\partial}{\partial r} + \frac{1}{r^2}\frac{\partial^2}{\partial \varphi^2})A_z \tag{37}$$

The current density is proportional to a $\cos\varphi$ factor so the magnetic field potential A_Z is expressed as a product of a radial function and $\cos\varphi$ [2, 36]. The following expressions are obtained [2, 36]:

$$A_z^1(r, \varphi) = \mu_0 H_{ext} \cos\varphi (r - \frac{c_1}{r}), r \geq r_{ext}, \tag{38}$$

$$A_z^2(r, \varphi) = \mu_0 H_{ext} \cos\varphi [c_2 I_1(kr) + c_3 K_1(kr)], r_{\text{int}} < r < r_{ext}, \tag{39}$$

$$A_z^3(r, \varphi) = \mu_0 H_{ext} c_4 r \cos\varphi, r \leq r_{\text{int}}, \tag{40}$$

where $I_1(\cdot)$ and $K_1(\cdot)$ are the first-order modified Bessel functions of the first and second kind, respectively. The unknown coefficients c_1, c_2, c_3 and c_4 can be determined using the boundary conditionsat the interface of the cylindrical shells, in a similar way as for the MSP. After solving the obtained algebraic linear system of equations, the unknown coefficients are determined. Using them the expressions of the magnetic vector potential in all of the three regions of interest can be obtained.

The shield effectiveness has the following expression [2]:

$$SE = \left| \frac{r_{\text{int}}}{2 r_{ext} \mu_r} \{[\mu_r K_1(k r_{int}) - k r_{int} K_1'(k r_{int})]\left[\mu_r I_1(k r_{ext}) + k r_{ext} I_1'(k r_{ext})\right] - [\mu_r I_1(k r_{int}) - k r_{int} I_1'(k r_{int})][\mu_r K_1(k r_{ext}) + k r_{ext} K_1'(k r_{ext})]\} \right| \tag{41}$$

where $I_1'(\cdot)$ and $K_1'(\cdot)$ are the first derivative of the first-order modified Bessel functions of the first and second kind, respectively.

The Eq. 41 has certain simpler forms for different conditions.

Considering the case when the radii of the shield are large compared to the skin depth (i.e. $r_{int}, r_{ext} = \delta$) a much simpler expression is obtained:

$$SE = \left| \begin{array}{l} \frac{\sqrt{r_{int}}}{8\mu_r k r_{ext}\sqrt{r_{ext}}}[k(r_{ext} + 8\mu_r r_{int} + 8\mu_r g)\cosh(kg) + \\ \left(kg + 4k^2 r_{int}^2 + k r_{int} + 4k^2 r_{int} g + 4\mu_r^2\right)\sinh(kg)] \end{array} \right| \tag{42}$$

For the case of a magnetic conducting thin shield, the following expression is obtained:

$$SE; \left|\cosh(\mathrm{kg}) + \frac{1}{2}\left(\frac{\mathrm{kr}_m}{\mu_\mathrm{r}} + \frac{\mu_\mathrm{r}}{\mathrm{kr}_m}\right)\sinh(\mathrm{kg})\right| \tag{43}$$

Considering the low-frequency approximation case, for the case of power applications ($|kg| = 1$) in (43), then the next expression is obtained:

$$SE; |1 + \frac{\mu_r}{2r_m} g + \frac{r_m}{2\mu_r} g k^2| \tag{44}$$

Considering the thick-shield approximation for the magnetic conducting cylindrical shell a different expression is derived, using the following approximations:

$$(|kg| = 1, r_m = \delta \text{ and } r_{ext}; r_{int} = r_0)$$

$$SE; |\frac{r_m k}{4\mu_r} e^{kg}| = \frac{r_m}{2\sqrt{2}\mu_r \delta} e^{g/\delta} \tag{45}$$

3 Finite Element Formulations for Magneto Static and Time Harmonic Magnetic Field

Problems of analysis of macroscopic electromagnetic field accept, out of the differential formulation, an equivalent variational approach.

In order to create the mathematical variational model of the electromagnetic field a variational principle (Lagrangian or Hemiltonian type) must be set. It must allow generating from a stationary condition of a certain functional (generally with a significance of electromagnetic energy) the fundamental equations of the electromagnetic field in material media [36, 37].

Numerical techniques convert the partial differential equations of the electromagnetic field in linear or non linear systems of algebraic equations. The solution of those systems generates an approximate solution of the electromagnetic

field in a discrete number of points of the field domain called nodes. Different approaches convert the PDEs that describe the field into a system of algebraic equations having as unknowns the values of the electric or magnetic potential. There different discretization techniques: finite difference method, finite element method, finite volume method, boundary element method.

The finite element method is recognized as a powerful and versatile method that can be used to a large class of engineering and mathematical problems, including those from electromagnetics.

The operation that named the method consists of discretization (mesh) of the 1D, 2D or 3D field domain into some 1D elements (line segments), 2D elements (triangles or quadrilaterals) and 3D elements (tetrahedrons, hexahedrons (bricks), as seen in Fig. 3a–d.

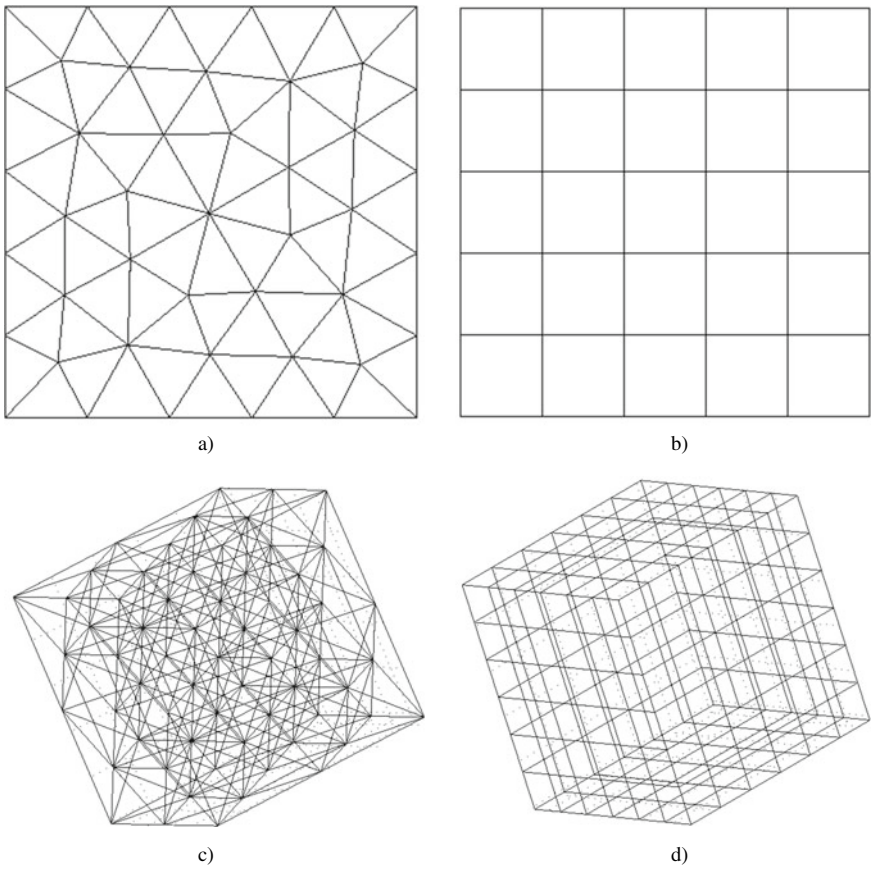

Fig. 3 Finite element discretizations **a** 2D structured mesh with squares **b** 2D unstructured mesh with triangle, **c** 3D non structured mesh with tetrahedrons, **d** 3D structured mesh with hexahedrons

Meshing with triangles and tetrahedron is called unstructured mesh. When quadrilaterals and hexahedrons (bricks) are used we are talking about structured mesh.

Then the unknown electromagnetic potentials at an elemental level are expressed as combinations of their values in the nodes of the mesh and a set of known functions called shape functions [36–38].

There are cases when the energy functional is very difficult to obtain or doesn't exist (generally for non-self adjointpartial differential equations PDEs). In those cases other techniques are used: the Ritz-Rayleigh and the Galerkin method.

They are not related with the minimization of a functional and can be used to solve directly the PDEs with boundary conditions.

The main computational steps that should be performed in order to solve a problem by the finite element method are:

- Discretizing the solution region into small sub domains called finite elements
- Obtaining the governing equation for a certain element (obtaining the element coefficient matrix)
- Assembling of all elements in the solution region (assembling all the elementary matrix into a global matrix, named stiffness matrix)
- Solving the resulting system of equations
- Post processing the results.

3.1 Finite Element Analysis of Magneto Static Field Using a Variational Formulation

We consider a plane-parallelmagnetostatic field, described by a Laplace equation, in 2D domain, having Dirichlet boundary conditionson the frontier Γ_2 [33–34, 36–39], (Fig. 4):

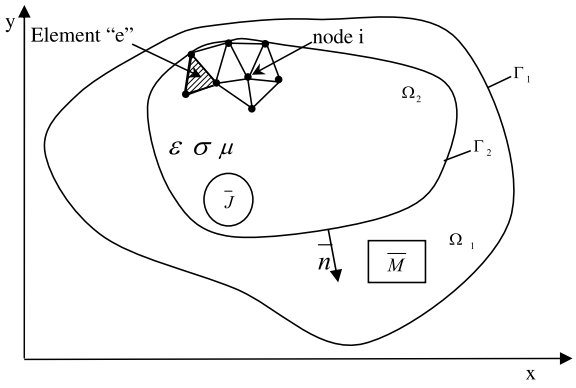

Fig. 4 Electromagnetic field domain

$$\nabla^2 A_z = 0 \tag{46}$$

where A_Z is the z component of the magnetic vector potential A, for this type of field.

Solving Eq. (46) is equivalent with obtaining the solution for a variational problem. It consists in finding the minimum of a certain functional, that represents the magnetic energy from the domain. This means that the distribution of the magnetic potential that satisfies the Laplace equation minimizes the magnetostatic energy from the domain.

The energy functional that corresponds to Eq. 46 has the following expression:

$$F(A) = \int_V \frac{1}{2\mu} \nabla^2 A_z dV \tag{47}$$

This equation presents the energy of the magnetic field from the respective domain. Solving the equation is simpler for plane-parallel or axisymmetricfields.

If we consider a parallel plane magnetic field in magnetostatic and assuming that the depth is in the Oz direction, the perpendicular on the field plane, equal with the unit, the functional. Using Eq. 47 can be written as a surface integral:

$$F(A) = \int_{S_{\Gamma_2}} \frac{1}{2\mu} \nabla^2 \overline{A} dS \tag{47'}$$

Being applied for each element, this transformation decreases the computational costs.

The application of the variational approach will be described as follows, considering a general electromagnetic media, described by parameters ε, σ and μ with magnetization domain $\overline{M}$ and current sources$\overline{J}$ (Fig. 4).

In the first step, the domain Ω_2 is split in smaller sub domains, called finite elements, with triangular shapes (Fig. 4). These elements can have different sizes, depending on the domain configuration, with the mesh density increasing where the field variation rate is higher. Let m be the total number of finite elements and n the total number of resulting nodes. By dividing the domain in a finite element mesh the functional Eq. 47 can be rewritten as the sum of the functionals corresponding to the m finite elements [34, 36]:

$$\Im = \sum_{e=1}^{m} \frac{1}{2\mu_e} \int_{S_e} (\nabla A_{ze})^2 ds \tag{48}$$

Expression (48) indicates that the method can be used to solve the magnetic field problems in heterogeneous domains that occur in practical situations.

Different finite elements can have different permeabilities (μ_{re}), the magnetic medium in a single element being homogenous. Also relation (48) indicates that, for

a linear media, the sum of the magnetostatic field energy from every finite element equals the whole magnetostatic field energy from domain Ω_2.

On the other hand, the use of the Eq. (48) instead of (47) should assume the fulfilling of specific interface conditions for the magnetostatic field at the interface between the adjacent finite elements.

For the magnetostatic field this means the continuity of the magnetic vector potentialA and the preservation of the normal components of the magnetic flux density at the interface between medium 1 and 2:

$$(B_n)|_{\mu_{r1}} = (B_n)|_{\mu_{r2}} \tag{49}$$

Usually polynomial approximations are used (Lagrange, Hermite).

Considering the finite elements small enough it could be considered that the magnetic vector potential (MVP) $A(x, y)$ has a linear variation with x and y, and can be described by a first degree algebraic polynom.

In Fig. 5 a current triangular finite element e, described by the nodes i, j, k with the coordinates $P_i(x_i, y_i)$, $P_j\left(x_j, y_j\right)$ and $P_k(x_k, y_k)$ is presented. For a point P inside the element (e), the MVP $A_z(x, y)$ can be written as follows [33, 40, 36]:

$$A_{ze} = \alpha_1 + \alpha_2 \cdot x + \alpha_3 \cdot y \tag{50}$$

or as a matrix:

$$A_{ze} = \begin{bmatrix} 1 & x & y \end{bmatrix} \cdot \begin{bmatrix} \alpha_1 \\ \alpha_2 \\ \alpha_3 \end{bmatrix} \tag{51}$$

For each element three coefficients should be computed.

Because the aim of the computing is to obtain the values of the magnetic potential in the nodes of the mesh then MVP A_{ze} should be expressed as a function of the magnetic potentials A_{zi}, A_{zj}, A_{zk} from the nodes i, j, k of the finite element "e", in

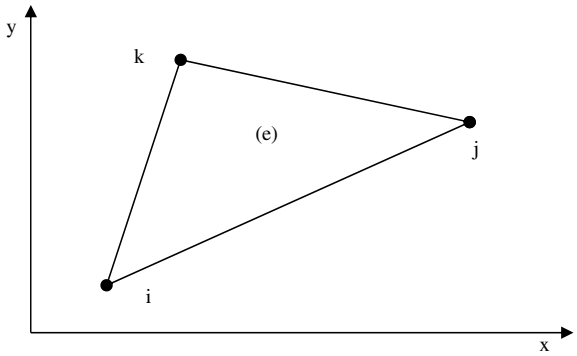

Fig. 5 First order triangular finite element

the following form:

$$A_{ze} = N_{ei} A_{zi} + N_{ej} A_{zj} + N_{ek} A_{zk} \tag{52}$$

or in a matrix form:

$$A_{ze} = \begin{bmatrix} N_{ei} & N_{ej} & N_{ek} \end{bmatrix} \cdot \begin{bmatrix} A_i \\ A_j \\ A_k \end{bmatrix} = [N] \cdot [A] \tag{53}$$

where the coefficients N_{ei}, N_{ej}, N_{ek} are linear functions of x and y, called shape functions. If the point P is in the node i the corresponding shape function has the value 1 and in the other is 0 $\left(N_{ej} = N_{ek} = 0\right)$.

This property can be described as $N_i(x_k, y_k) = \delta_{ik}$, where δ_{ik} is the symbol of Kronecker.

For two adjacent elements the value of the magnetic potential in the common nodes is equal. In order to improve the precision, higher degree polynomials can be used.

For example in Fig. 6, for each side another node has been added in a second order polynomials approach. The magnetic potential has the following expression:

$$A_e = \alpha_1 + \alpha_2 x + \alpha_3 y + \alpha_4 x^2 + \alpha_5 xy + \alpha_6 y^2 \tag{54}$$

respectively:

$$A_e = N_{ei} A_i + N_{ej} A_j + N_{ek} A_k + N_{ea} A_a + N_{eb} A_b + N_{ec} A_c \tag{55}$$

For each element six coefficients should be computed. The precision is higher, but the execution time increases.

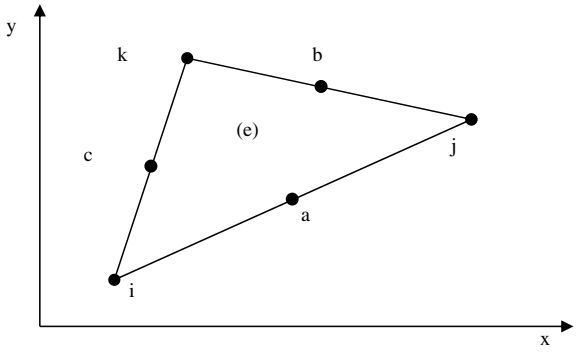

Fig. 6 Second order triangular finite element

In order to increase the accuracy of the finite element solution usually three strategies are used.

The first one is the h-version of the finite element that uses low polynomial degree (i.e. p = 1, 2) and increases the mesh density. With this approach the approximation error decreases algebraically versus the number of the unknowns.

The second technique is to maintain the mesh density and to increase the degree p of the approximation polynomial. This is the p version of the finite element method. For simpler cases, when the solution is smooth, this approach has an exponential convergence versus the number of unknowns. For the practical cases the convergence rate is algebraic. The exponential convergence can be reached again using the hp-version of the finite element method.

The shape functions will be determined for a linear approximation. Writing the Eq. 51 for nodes i, j, k the following matrix expression is obtained:

$$[A] = \begin{bmatrix} 1 & x_i & y_i \\ 1 & x_j & y_j \\ 1 & x_k & y_k \end{bmatrix} \cdot \begin{bmatrix} \alpha_1 \\ \alpha_2 \\ \alpha_3 \end{bmatrix} \tag{56}$$

Solving the system in Eq. 56 we obtain the coefficients $\alpha_1, \alpha_2, \alpha_3$

$$\begin{bmatrix} \alpha_1 \\ \alpha_2 \\ \alpha_3 \end{bmatrix} = \begin{bmatrix} 1 & x_i & y_i \\ 1 & x_j & y_j \\ 1 & x_k & y_k \end{bmatrix}^{-1} \cdot \begin{bmatrix} A_{zi} \\ A_{zj} \\ A_{zk} \end{bmatrix} \tag{57}$$

The vector of the shape functions is then:

$$[N_e] = \begin{bmatrix} 1 & x & y \end{bmatrix} \cdot \begin{bmatrix} 1 & x_i & y_i \\ 1 & x_j & y_j \\ 1 & x_k & y_k \end{bmatrix}^{-1} \tag{58}$$

The determinant of the second matrix from the r.h.s. is equal with $2S_e$ where S_e is the area of the triangle e. The following relations for the shape functions are obtained [33, 40]:

$$\begin{aligned} N_{ei} &= \frac{1}{2S_e}\left(x_j y_k - x_k y_j\right) + \left(y_j - y_k\right)x + \left(x_k - x_j\right)y \\ N_{ej} &= \frac{1}{2S_e}(x_k y_i - x_i y_k) + (y_k - y_i)x + (x_i - x_k)y \\ N_{ek} &= \frac{1}{2S_e}\left(x_i y_j - x_j y_i\right) + \left(y_i - y_j\right)x + \left(x_j - x_i\right)y \end{aligned} \tag{59}$$

After doing the calculation the following expression for the gradientof the magnetic potential is obtained:

$$grad\, A_{ze} = \bar{i}\frac{\partial A_{ze}}{\partial x} + \bar{j}\frac{\partial A_{ze}}{\partial y} = \bar{i}\frac{\partial}{\partial x}\left(N_{ei}A_{zi} + N_{ej}A_{zj} + N_{ek}A_{zk}\right) + \bar{j}\frac{\partial}{\partial y}\left(N_{ei}A_{zi} + N_{ej}A_{zj} + N_{ek}A_{zk}\right) \tag{60}$$

If we take into account Eq. 59 then Eq. 60 becomes:

$$grad\, A_{ze} = \bar{i}\frac{1}{2S_e}\left[\left(y_j - y_k\right)A_{zi} + (y_k - y_i)A_{zj} + \left(y_i - y_j\right)A_{zk}\right] + \bar{j}\frac{1}{2S_e}\left[\left(x_k - x_j\right)A_{zi} + (x_i - x_k)A_{zj} + \left(x_j - x_i\right)A_{zk}\right] \tag{61}$$

Considering for each element that $|grad\, V| = const$ then the functional Eq. 48 becomes [33]:

$$\Im = \sum_{e=1}^{m} \frac{\mu_e S_e}{2} \cdot (\nabla A_{ze})^2 \tag{62}$$

and it be can be rewritten as:

$$\Im = \sum_{e=1}^{m} \frac{\mu_e}{8S_e}\left\{\begin{array}{l}\left[\left(y_j - y_k\right)A_{zi} + (y_k - y_i)A_{zj} + \left(y_i - y_j\right)A_{zk}\right]^2 \\ +\left[\left(x_k - x_j\right)A_{zi} + (x_i - x_k)A_{zj} + \left(x_j - x_i\right)A_{zk}\right]^2\end{array}\right\} \tag{63}$$

The functional Eq. 62 has been transformed into a function that has as variables the magnetic potentials in the n nodes of the field domain.

Minimization of it is obtained imposing in each nodal point i that the derivative in relation to A_{zi} to be 0:

$$\frac{\partial \Im}{\partial A_{zi}} = 0, \mathrm{i} = 1, 2, \ldots, \mathrm{n} \tag{64}$$

and a system with n algebraic equations that has n unknowns, the magnetic potentials in nodes i, is obtained:

$$[C][A] = [b] \tag{65}$$

If the boundary conditions are of Dirichlet type, given the potentials in the nodes of the domain frontier, the total number of variables is less than n, but even in this case it is equal to the number of equations.

In many engineering applications matrix C, the stiffness matrix, is symmetrical and sparse and band structured. The equation system is numerically solved, giving the potential values for the nodes. For 2D problems direct solvers are used and for 3D problems iterative solvers are indicated.

In the postprocessor module, for each finite element we can compute ($grad\ A_{z\lambda}$) as well as the field vector.

The finite element method is a discretization method for field computing, as is the finite differences method, which is suitable to be compared with. While the finite differences method is based on equation approximation with partial derivates by using finite differences equations, the finite element method approximates the potential function for a finite element. Both methods, as well as the boundary element method, lead to an algebraic system of equations where the unknowns are the potentials of the nodes. In the case of boundary elements method the resulting matrix is fully populated.

The finite element method has advantages in certain situations. Thus, it can be used for complex geometrical configurations, for linear and non linear PDEs, for coupled problems (electro-thermal, magneto-structuraland electromagnetic field electric circuits), varying materials and boundary conditions and anisotropicmaterials.

3.2 *Finite Element Galerk in Formulation a Time Harmonic Magnetic Field*

The time magnetic dependent field problems are also referred as eddy current problems. They occur in the cases of the electromagnetic shields.

There are many situations that require solutions of the time harmonic problems, such as: AC electric machines, electromagnetic shields, transformers, magnetic brakes. In the quasi stationary regime, the density of the displacement current is neglected in relation to density of the conduction current $\overline{J_D} = \frac{\partial \overline{D}}{\partial t} = \overline{J} = \sigma \overline{E}$.

The equation of the quasi stationary electromagnetic field for the magnetic vector potentials [35, 38, 41] is the following:

$$\nabla \cdot \frac{1}{\mu} \nabla \overline{A} = \sigma \frac{\partial \overline{A}}{\partial t} + \overline{J_S} \tag{66}$$

where $\overline{J_S}$ is the excitation current and for the linear media:

$$\Delta \overline{A} = \mu \sigma \frac{\partial \overline{A}}{\partial t} + \mu \overline{J_S} \tag{67}$$

For 2D problems the MVP A has only one component A_Z that satisfies the Coulomb gauge and the Eq. (66) becomes:

$$\nabla \cdot \frac{1}{\mu} \nabla \overline{A_z} = \sigma \frac{\partial \overline{A_z}}{\partial t} + \overline{J_{sz}} \tag{68}$$

For the time harmonic steady state regime the complex representation of the MVP A can be obtained using the exponential form:

$$\underline{A} = Ae^{j\omega t} \tag{69}$$

where ω is the angular frequency and j is the imaginary unit.

If we substitute Eq. (69) in Eq. (67), we obtain [40, 34, 36–38]:

$$\nabla \cdot \frac{1}{\mu} \nabla \overline{A} - j\sigma\omega A = \overline{J_S} \tag{70}$$

The solution of Eq. 70 is defined into a finite domain D, subjected to boundary conditions on the frontier Γ. The most encountered boundary conditions require either the normal or the tangential magnetic flux density to be zero respectively.

In terms of MVPA they are equivalent with the following homogenous boundary conditions:

$$\frac{\partial A}{\partial n} = 0 \tag{71}$$

$$\mathrm{A} = 0 \tag{72}$$

We'll apply the weighted residual methodto Eq. 70. In order to satisfy the compatibility condition at the interface at two adjacent finite elements we'll consider shape functions with C_0 continuity. After applying the first Green identity the following relation is obtained [40, 36, 38]:

$$-\int_{\Omega} \nabla w_i \frac{1}{\mu} \nabla \underline{A} d\Omega + \int_{\Gamma} w_i \frac{\partial \underline{A}}{\partial n} d\Gamma - \int_{\Omega} w_i (j\omega\sigma A + J_S) d\Omega = 0 \tag{73}$$

Using the basis functions, the magnetic vector potential can be expressed at elemental level as follows:

$$\underline{A} = \sum N_i \underline{A_i} \tag{74}$$

where for triangular linear elements the shape functionsN_i are:

$$N_i = \frac{a_i + b_i x + c_i y}{2A} \tag{75}$$

where A is the area of an element with the nodes i, j and k.

If we set the shape functions to be the weighted functions$w_i = N_i$, then the weighted residual method becomes the Galerkin method. The discretized form of Eq. 73, at elemental level, becomes:

$$\left[\int_{elem}\frac{1}{\mu}\left(\frac{\partial N_i}{\partial x}\frac{\partial N_j}{\partial x}+\frac{\partial N_i}{\partial y}\frac{\partial N_j}{\partial y}\right)dxdy-j\int_{elem}\sigma\omega N_iN_jdxdy\right]\cdot[A_i]=\left[\int_{elem}N_iJ_Sdxdy\right] \tag{76}$$

The latter equation can be written in the form of an algebraic system of equations:

$$\left[\underline{k}\right]\cdot\left[\underline{A}\right]=\left[\underline{Q}\right] \tag{77}$$

For the linear triangular finite element elements, the coefficients matrix k_{ij} can be represented as [40]:

$$\underline{k_{ij}}=\underline{p_{ij}}+j\underline{q_{ij}} \tag{78}$$

The real part p_{ij} is described by:

$$p_{\mathrm{ij}}=\frac{1}{4A\mu}\left(\mathrm{b_ib_j}+\mathrm{c_ic_j}\right) \tag{79}$$

and using the Holland- Bell formula [35–37]:

$$\int N_1^aN_2^bN_3^cd_\Omega=2A\frac{a!b!c!}{(a+b+c+2)!} \tag{80}$$

we obtain for q_{ij} the following expression:

$$q_{\mathrm{ij}}=-\sigma\mu\int_{elem}N_iN_jdxdy=\frac{A\sigma\omega}{12}\begin{bmatrix}2&1&1\\1&2&2\\1&1&2\end{bmatrix} \tag{81}$$

where A is the area of the triangular element.

In order to obtain the global matrix, the elemental matrices must be assembled.

The matrix from Eq. 77 is symmetric and the coefficients are complex. The extra time needed to solve an eddy current problem by comparison with magnetostatics case is due to the required time to perform the computations using complex numbers.

The Galerkin method is one of the most versatile methods used for the numerical solution of the PDEs.

4 Case Study: Determination of the Magnetic Field Produced by a High Voltage Electrical Overhead Line Near a Shielded Building Using Finite Element Method

The influence of overhead transmission lines represents a thematic of real interest in the domain of transport of power because it is possible to have an impact on the human body. This application proposes a calculation model of the magnetic field in harmonic regime produced by the high voltage conductors of the transmission systems of electricity using the finite element method. The numerical computation of magnetic field in the vicinity of a high voltage 220 kV electrical overhead line is analyzed. To calculate the magnetic field strength and the magnetic flux density near the overhead power line and the shielded building, the ANSYS Multiphysics software package is used.

The magnetic field strength at ground level depends on the distance to the line and the currents intensity, which flows in the phase conductors. Unlike voltage, the intensity of the electric current can vary very quickly during a day and depending on the season. The intensity of this field depends also on the height and spatial distribution of the conductors. There are other sources (on a small scale) that contribute to the intensity of the magnetic field: currents from the neutral conductor, currents induced in the protective conductors of overhead line, currents in the adjacent ground, in the telecommunications circuits, in pipes or other metallic structures, which it was parallel to the overhead line.

In the literature there are some studies containing an analytical calculation of the magnetic field caused by high voltage power lines. Different techniques can be applied for the calculation of the magnetic field produced by the electrical lines supported by poles of unequal height, unequal distances between poles and or poles whose arrangement is not linear [42]. In another paper, the authors set out to develop a method of calculating the magnetic field generated by conductors arranged in different geometries for single and double circuit electrical lines. For example, in [43], a method of calculating the magnetic field in the vicinity of an electric line called complex double numbers is developed for the following configurations: flat and vertical power lines, lines with polygonal symmetry, delta power line, lines in hexagonal arrangement. The attenuation of the magnetic field created by a double circuit electrical line can also be achieved through an optimization of the arrangement of the phase conductors that feed a railway station and a distribution station [44].

The numerical integration of the Biot-Savart law in differentiated form represents the main analytical method for calculating the density of the magnetic flux [45]. The magnetic field produced by electric power lines is usually calculated numerically with the use of a computer. In [46] specific calculations of the magnetic field for an 110 kV overhead line are presented. In [47] the effect of harmonic components at different electromagnetic frequencies is also taken into account. In [48] historical load databases are used to take into account the relations between magnetic field and electrical load patterns. In [49], 50 the magnetic field distribution is calculated and measured in high voltage substations. To reduce the low-frequency magnetic field in

a building near a high-voltage power line the building is screened with materials that modify its distribution. The shielding factor depends on the permeability, geometry, and thickness of the material [51, 52].

In this application, the magnetic field is calculated using finite elements method (FEM) generated by the conductors of a high voltage electrical line in an area near a building, located in the electric station. The six conductors of a 220 kV transposed high voltage transmission line with double circuit are considered. Consider a system consisting of 6 conductors (double circuit) with 3 conductors on each circuit. The conductors are located at a height of 15 m from earth. Each conductor has a diameter of 30 mm and is located at a distance of 3.6 m and 5 m (central conductors) of the pole of power line. The building is made of concrete with magnetic permeability 1, with a length of 10 m and a height of 6 m, located at a distance of 15 m from the central axis of the conductors. At the top of the building there is a steel screen. Two types of steel with different magnetic permeability of 1000, 4000 and 10,000 respectively were considered. The screen has a length of 11 m and a thickness of 5 mm. Figure 7 shows the physical model consisting of the six conductors and the shielded building and in Fig. 8 is presented a detail that includes the shielded building. The building is surrounded on the outside with a screen with a thickness of 3 mm and in addition to the floor of the building there is a screen of 3 mm. Between the two screens in the floor there is a 4 mm air gap.

The power lines are the conductors of Aluminum Conductor Steel Reinforced (ACSR) type, having the magnetic permeability $\mu_r = 300$ [53, 54]. The conductors are crossed by currents of 375 A, phase shifted by 120° on the three phases. The simulation was done in harmonic mode.

After creating the physical model and define materials, the next step in the preprocessor phase is mesh generation and load applying upon the elements. The finite element mesh of the system with six conductors is shown in Fig. 9. We used a mesh with 314,548 nodes and 628,593 triangular elements. In Fig. 10 is presented the discretization mesh for the shielded building. The boundary conditions and loads to

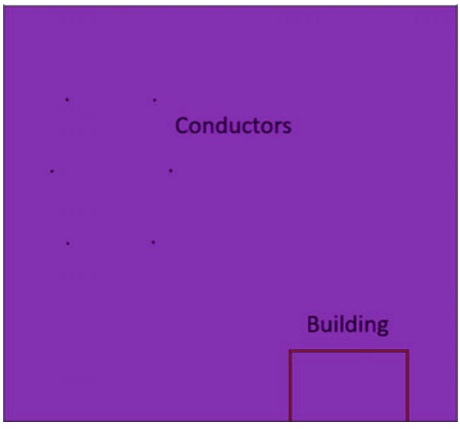

Fig. 7 The physical model subjected to modeling

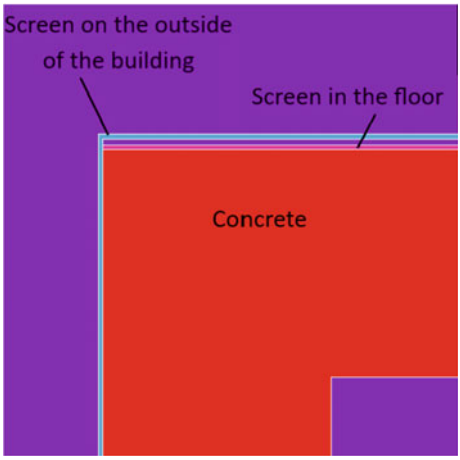

Fig. 8 The physical model comprising the shielded building

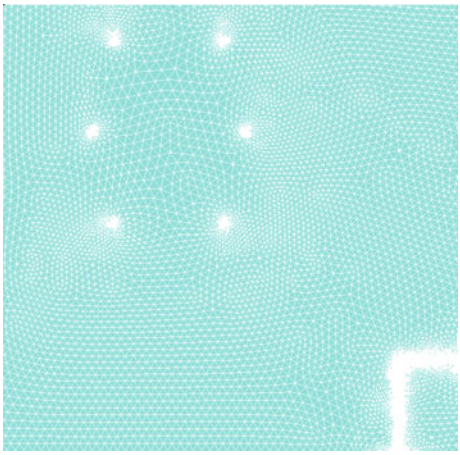

Fig. 9 Finite element mesh

a 2D harmonic magnetic field analysis are applied, both on the plane model (key points, lines, and areas) and on the finite element model (nodes and elements) [55]. The solution of magnetic field problems is commonly obtained using potential functions. Depending on the problem to be solved, one of the two types of potential functions, the MVPor the MSP, is used.

Figure 11 shows the distribution of the magnetic field around the six conductors and shielded building. The maximum value of the magnetic field intensity is obtained around the conductors. In this region, the magnetic field intensity has a maximum of 3403.14 A/m. Inside the building, the intensity of the magnetic field has values between 8.35 and 3.25 A/m for the steel shielded building with magnetic permeability 1000 and between 7.25 and 2.7 A/m for the steel shielded building with the permeability 4000. These values are obtained at a distance of 1.8 m from the ground.

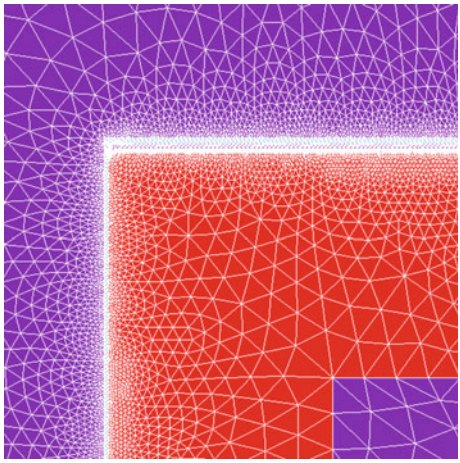

Fig. 10 Finite element mesh (detail building shielded)

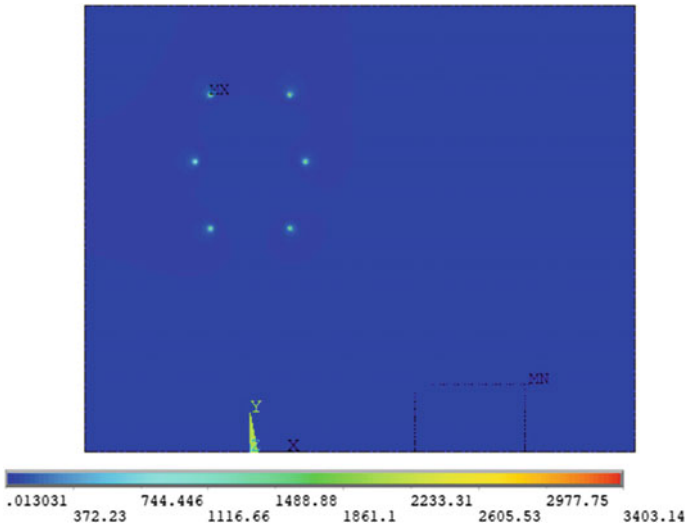

Fig. 11 Distribution of the magnetic field around the conductors and shielded building

Ata distance of 4.8 m from the ground, the maximum values of the magnetic field intensity are 9.37 A/m for the shielded building, with 1000 magnetic permeability steel and 9.06 A/m for the shielded building with 4000 magnetic permeability steel.

The distribution of magnetic flux density all over the surface is shown in Fig. 12 and the distribution of magnetic flux density around the conductor is presented in Fig. 13. The two reference distances were chosen for the evaluation of the magnetic

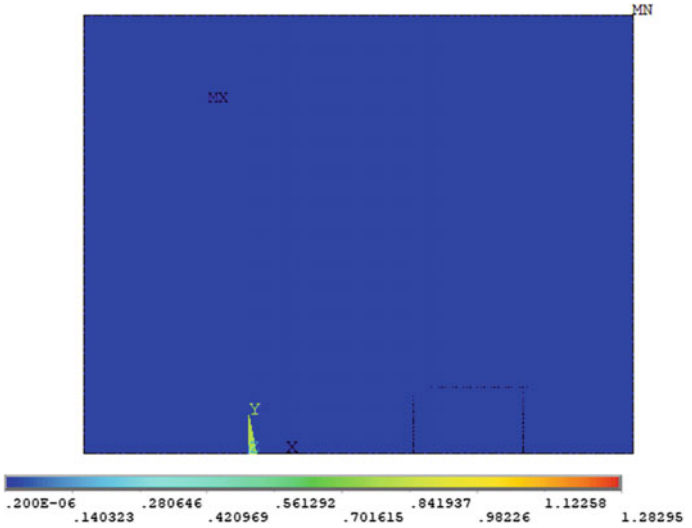

Fig. 12 The distribution of magnetic flux density around the conductors and shielded building

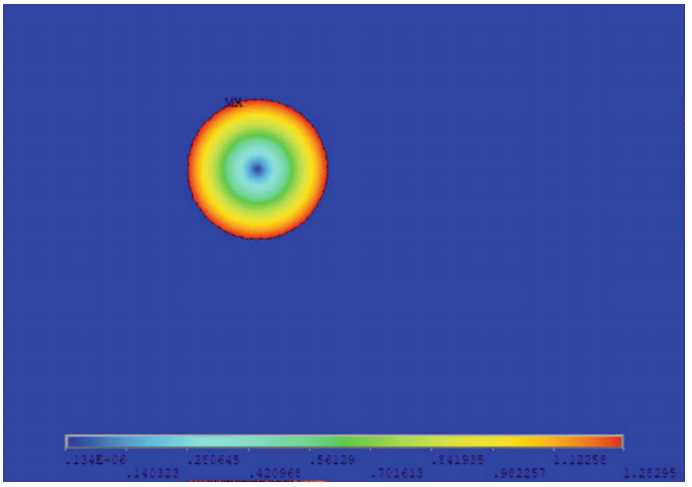

Fig. 13 The distribution of magnetic flux density around the conductor

sizes of 1.8 m and 4.8 m respectively, which means the distance at the head level for the persons on the ground floor and respectively on the floor.

The magnetic induction has values between 9.23 and 2.19 μT for the screen with the magnetic permeability 1000 and 3.64 and 1.09 μT for the screen with the magnetic permeability 4000. These values were obtained on the contour drawn at a distance of 1.8 from the ground.

At a distance of 4.8 m were recorded values between 9.62 and 4.16 μT in the case of the screen with magnetic permeability 1000 and 4.74 and 2.12 μT in the case of the screen with magnetic permeability 4000.

The maximum value of the magnetic flux density is obtained around the conductors. In this region, the magnetic flux density has a maximum of 1.282 T for the conductors traversed by a current of 375 A.

In ANSYS there is a graphical program that displays the resulting fields in the form of contour and density plots. The path for the displayed charts is chosen on a contour consisting of two points placed symmetrical from the shielding building.

Figure 14 and Fig. 15 show the chart of the magnetic flux density inside the building, at 1.8 m and 4.8 m above the ground, respectively. Screening is more efficient when using a material with higher magnetic permeability. In Figs. 16 and 17 represented the values of the magnetic induction in the case of shielding with ferromagnetic steel with magnetic permeability 10,000. It was considered the case

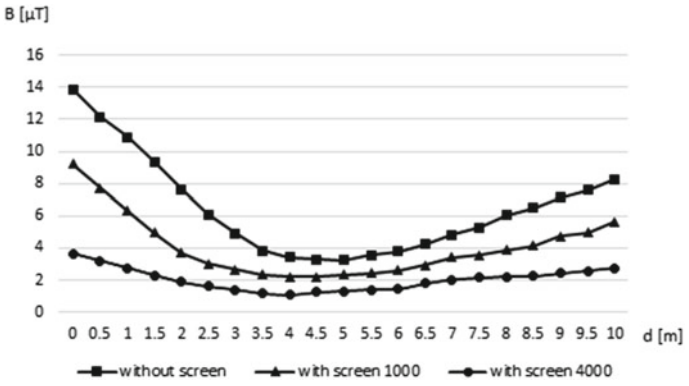

Fig. 14 Chart of magnetic flux density inside the building, at a distance of 1.8 m

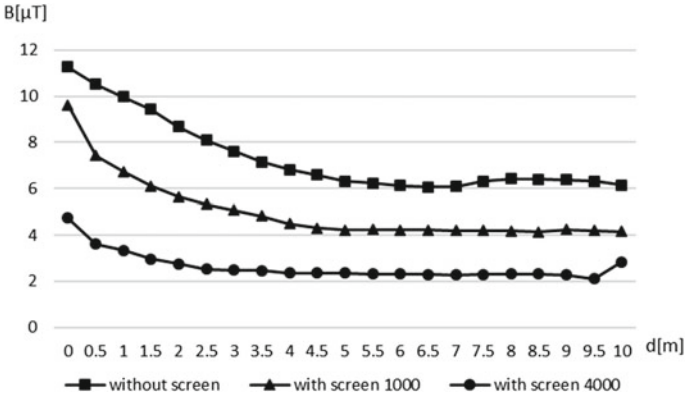

Fig. 15 Chart of magnetic flux density inside the building, at a distance of 4.8 m

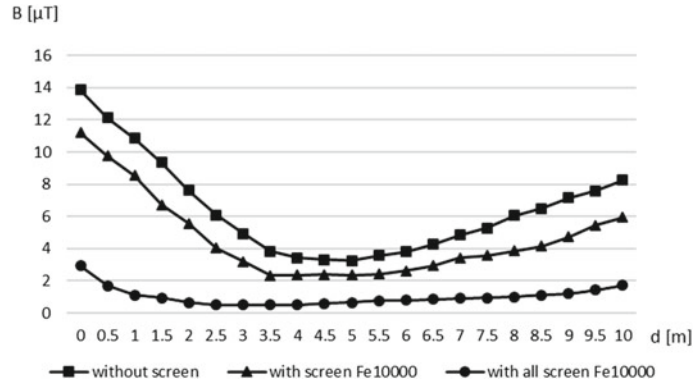

Fig. 16 Chart of magnetic flux density inside the building, at a distance of 1.8 m

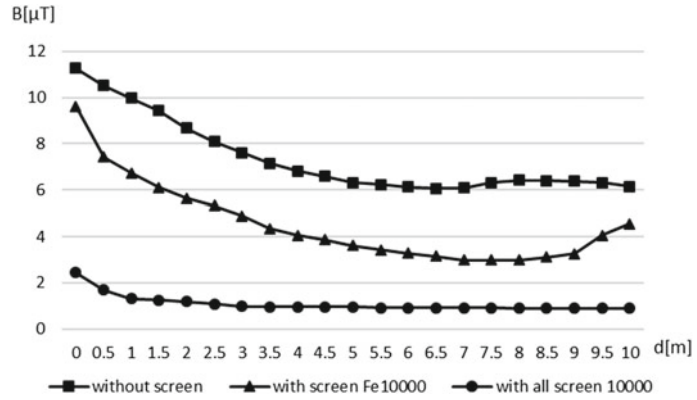

Fig. 17 Chart of magnetic flux density inside the building, at a distance of 4.8 m

of the screen only in the floor of the building (with screen Fe 10,000) but also the complete screen outside the building and in the floor (with all screen Fe 10,000), for those two distances. It is found that the screen only of the floor is not efficient, the values of the magnetic field in this case being comparable with those existing in the absence of the screen. The obtained values are within the limits imposed by ICNIRP standards [56].

5 Conclusions

In this paper, we presented the calculation of the magnetic field produced by a high voltage electrical overhead line in a nearby building located in the electrical station. Screening is efficient when using multi-layer screens made of materials with

the highest magnetic permeability. In the case of complete shielding with 10,000 ferromagnetic steel with magnetic permeability, magnetic induction values below 2 μT were obtained.

Different materials and multi-layer passive shields will be considered in the future. Also, active shields will be considered.

The presented method can be useful in the design of a transmission power lines for insulation distance estimation. Finite element numerical simulation approach can be used to predict the magnetic field generated by high voltage overhead power lines. It can also be used for evaluation of the shielding techniques used for SLF magnetic flux mitigation.

References

1. Bravo JC, del Pino LJ, Cruz P (2019) A survey on optimization techniques applied to magnetic field mitigation in power systems. Energies 12:1332. https://doi.org/10.3390/en12071332
2. Celozzi S, Araneo R, Lovat G (2008) Electromagnetic shielding. Wiley, Inc. https://doi.org/10.1002/9780470268483
3. Fireteanu V, Popa M, Tudorache T (2004) Modele Numerice in Studiulsi Conceptia Dispozitivelor Electrotehnice (publication in Romanian). MatrixRom, Bucharest Romania
4. Salinas E (2001). Mitigation of power-frequency magnetic fields: with applications to substations and other parts of the electric network. PhD thesis, Chalmers University of Technology Göteborg, Sweden, https://publications.lib.chalmers.se/records/fulltext/523/523.pdf. Accessed 10 Jan 2019
5. Zhao Y, Sun Z, Pan D, Lin S, Jin Y, Li L (2019) A new approach to calculate the shielding factor of magnetic shields comprising nonlinear ferromagnetic materials under arbitrary disturbances. Energies 12:2048. https://doi.org/10.3390/en12112048
6. Yang J, Zhang W, Zou L, Wang Y, Sun Y, Feng Y (2019) Research on distribution and shielding of spatial magnetic field of a DC air core smoothing reactor. Energies 12:937. https://doi.org/10.3390/en12050937
7. Cazacu D, Enescu F, Castravete S (2013) Numerical problems in 3D FEM simulation of harmonic magnetic fields. In: 2013 international conference on electronics, computers and artificial intelligence, ECAI 2013, pp 1–4. https://doi.org/10.1109/ECAI.2013.6636193
8. Cazacu D (2013) Numerical problems in 3D magnetostatic FEM analysis. In: 15th WSEAS international conference on automatic control, modelling and simulation ACMOS '13. Brasov, Romania, pp 385–390
9. Cazacu D, Castravete S (2012) Efficiency evaluation via finite element method of 3D magnetostatic shields using different types of magnetic potentials, pp 25–30. https://doi.org/10.1109/SIITME.2012.6384340
10. Cazacu D, Stoica C (2015) Teaching computational aspects on the efficiency of multi layer spherical magneto static shields. In: Proceedings of the 2014 6th international conference on electronics, computers and artificial intelligence, ECAI 2014, pp 59–64. https://doi.org/10.1109/ECAI.2014.7090199
11. Cazacu D (2012) Factors that influence the magnetostatic shields effectiveness. Bull Electr Eng Faculty, Valahia Univ Tirgoviste 1:6–11
12. Cazacu D, Ionescu V, Ionita S, Virjoghe E (2016) On the multishell cylindrical magnetostatic shields: analytical and numerical approach, pp 1–4. https://doi.org/10.1109/ECAI.2016.7861092
13. Cazacu D, Stanescu C (2008) Finite element models of a transmission line for a plane electromagnetic wave in a shielding material. In: The 1st WSEAS international conference on finite differences, finite elements, finite volumes, boundary elements. Malta, pp 117–121

14. Stanescu C, Cazacu D (2008). Experimental and numerical aspects concerning the electromagnetic shielding materials. In: Proceedings of the 4th international conference on technical and physical problems of power engineering. Pitesti, Romania, pp 150–156
15. Virjoghe EO, Băncuţă I, Husu AG, Cazacu D, Florescu V (2019) Measurement and numerical modelling of electric field in open type air substation. J Sci Arts 19(1):249–259
16. Ionescu V, Cazacu D (2016) Analysis of COMSOL multiphysics parallel performance on a multi-core system, pp 1–5. https://doi.org/10.1109/ICATE.2016.7754605
17. Ionescu VM, Cazacu D (2015) Virtualization impact on comsol processor detection. Univ Pitesti Scienti Bull, Series Electron Comput Sci 15(2):25–32
18. Cazacu D, Jubleanu R, Bizon N, Monea C (2019) Comparative numerical analysis of the stored magnetic energy in cylindrical and toroidal superconducting magnetic coils. In: Proceedings of the 2019 11th international conference on electronics, computers and artificial intelligence (ECAI). Pitesti, Romania. https://doi.org/10.1109/ECAI46879.2019.9042162
19. Êvo M, de Paula H, Lopes I, Mesquita R, Souza D (2017) Study of the influence of underground power line shielding techniques on its power capability. J Control Automat Electr Syst 28:1–11. https://doi.org/10.1007/s40313-017-0319-x
20. Ates K, Carlak F, Ozen S (2016) Magnetic field exposures due to underground power cables: a simulation study. https://doi.org/10.11159/eee16.133
21. Li J, Quan W, Han B, Liu F, Xing L, Liu G (2018) Multilayer cylindrical magnetic shield for SERF atomic co-magnetometer application. IEEE Sens J 1–1. https://doi.org/10.1109/JSEN.2018.2890083
22. Sankaran K (2019) Recent trends in computational electromagnetics for defence applications. Defence Sci J 69:65–73. https://doi.org/10.14429/dsj.69.13275
23. Mu L (2019) Weak Galerkin based a posteriori error estimates for second order elliptic interface problems on polygonal meshes. J Comput Appl Mathemat 361. https://doi.org/10.1016/j.cam.2019.04.026
24. Wang C, Wang J (2019) Primal-dual weak Galerkin finite element methods for elliptic Cauchy problems. Comput Mathemat Appl 79(3):746–763. https://doi.org/10.1016/j.camwa.2019.07.031
25. Hortopan G, Vlase O, Nitu S (1990) Ecranarea Electromagntica in Tethnica Curentilor Intensi (publication in Romanian). Ed Tehnica, Bucharest
26. Kou Y, Jin K, Zheng X (2011) Numerical simulation on the shielding efficiency of magnetic shielding enclosures in the ITER applications. Comput Mater Continua 22:129–146
27. Yashchuk V, Lee S, Paperno E (2013) Magnetic shielding. In: Budker D, Kimball DJ (eds) Optical magnetometry. Cambridge University Press, Cambridge, pp 225–248. https://doi.org/10.1017/CBO9780511846380.013
28. Whelan B, Kolling S, Oborn BM, Keall P (2018) Passive magnetic shielding in MRI-Linac systems. Phys Med Biol 63(7):075008
29. Hoburg JF (1995) Principles of quasistatic magnetic shielding with cylindrical and spherical shields. IEEE Trans Electromag Compat 37(4):574–579. https://doi.org/10.1109/15.477342
30. Hortopan G (2005) Principii si Tehnici de Compatibilitate Electromagnetica (publication in Romanian). Editura Tehnica, Bucharest
31. Losito O, Dimiccoli V, Barletta D (2011) Low frequency shielding improvement by multilayer design. In: Proceedings of EMC Europe 2011 York—10th international symposium on electromagnetic compatibility, pp 640–643
32. Lipworth G, Ensworth J, Seetharam K, Lee J, Schmalenberg P, Nomura T, Reynolds M, Smith D, Urzhumov Y (2015) Quasi-static magnetic field shielding using longitudinal Mu-near-zero metamaterials. Scienti Rep 5:12764. https://doi.org/10.1038/srep12764
33. Sora C (1982) Bazele Electrotehnicii (publication in Romanian). Editura Didacticasi Pedagogica, Bucharest
34. Kaiser KL (2006) Electromagnetic shielding. Taylor & Francis
35. Mocanu CI (1981) Teoria Campului Electromagnetic (publication in Romanian). Editura Didacticasi Pedagogica, Bucharest
36. Polyak D (2007) Advanced modelling in computational electromagnetic compatibility. Wiley

37. Mindru G, Radulescu M (1986) Analiza Numerica a Campului Electromagnetic (publication in Romanian). Dacia Publishing House, Bucharest
38. Jin JM (2010) Theory and computation of electromagnetic fields. Wiley
39. Humphries S Jr (1997) Finite element methods for electromagnetics. CRC Press
40. Binns KJ, Lawrenson PJ, Trowbridge CV (1992) The analytical and numerical solution of electric and magnetic fields. Wiley
41. Kuczmann M (2009) Potential formulations in magnetic applying the finite element method. https://maxwell.sze.hu/docs/C4.pdf. Accessed 22 Feb 2019
42. El Dein A (2009) Magnetic-field calculation under EHV transmission lines for more realistic cases. IEEE Trans Power Delivery 24:2214–2222. https://doi.org/10.1109/TPWRD.2009.2028794
43. Filippopoulos G, Tsanakas D (2005) Analytical calculation of the magnetic field produced by electric power lines. IEEE Trans Power Delivery 20:1474–1482. https://doi.org/10.1109/TPWRD.2004.839184
44. Molnar-Matei F, Andea P, Pană A, Teslovan R (2012) Double circuit 110 kV overhead line magnetic field analysis, pp 780–783. https://doi.org/10.1109/MELCON.2012.6196546
45. Andreuccetti D, Zoppetti N, Conti R, Fanelli N, Giorgi A, Rendina R (2003) Magnetic fields from overhead power lines: advanced prediction techniques for environmental impact assessment and support to design, vol 2, 7 pp. https://doi.org/10.1109/PTC.2003.1304684
46. Lunca E, Istrate M, Salceanu A, Tibuliac S (2012) Computation of the magnetic field exposure from 110 kV overhead power lines. In: EPE 2012—proceedings of the 2012 international conference and exposition on electrical and power engineering, pp 628–631. https://doi.org/10.1109/ICEPE.2012.6463803
47. Okrainskaya I, Sidorov AI, Gladyshev SP (2012) Electromagnetic environment under over head power transmission lines 110–500 kV, pp 796–801. https://doi.org/10.1109/SPEEDAM.2012.6264574
48. Mazzanti G (2010) Evaluation of continuous exposure to magnetic field from AC overhead transmission lines via historical load databases: common procedures and innovative heuristic formulas. IEEE Trans Power Delivery 25:238–247. https://doi.org/10.1109/TPWRD.2009.2035390
49. Munteanu C, Pop, LT, Tapa V, Hangea C, Gutiu T, Lup S (2012) Study of the magnetic field distribution inside very high voltage substations, pp 660–663. https://doi.org/10.1109/ICEPE.2012.6463571
50. Aponte G, Cadavid H, Perez R, Escobar A, Mora A, Bolanos H (2003) Electric and magnetic fields measured in Colombian lines and substations, vol 2, pp 1195−1198. https://doi.org/10.1109/ICSMC2.2003.1429132
51. Beiu C, Golovanov N, Cornel T, Buica G (2017) Low frequency electromagnetic shielding solutions. https://doi.org/10.1109/SIELMEN.2017.8123301
52. Livesey K, Camley R, Celinski Z, Maat S (2017) Magnetic shielding of 3-phase current by a composite material at low frequencies. AIP Adv 7:056328. https://doi.org/10.1063/1.4978702
53. Andrei H, Fluerașu C, Vîrjoghe EO, Fluerașu C, Enescu D, Popovici D, Husu AG, Andrei PC, Predușcă G, Diaconu E (2011) Numerical methods, modelling and simulation applied in electrical engineering. Ed. Electra, Bucharest
54. Tupsie S, Isaramongkolrak A, Pao-la-or P (2010) Analysis of electromagnetic field effects using FEM for transmission lines transposition. Int J Electr Comput Eng 5(4):713–717
55. Salari J, Mpalantinos A, Silva JI (2009) Comparative analysis of 2- and 3-D methods for computing electric and magnetic fields generated by overhead transmission lines. IEEE Trans Power Delivery 24:338–344
56. Lin J, Saunders R, Schulmeister K, Söderberg P, Stuck BE, Swerdlow A, Taki M, Veyret B, Ziegelberger G, Repacholi M, Matthes R, Ahlbom A, Jokela K, Roy C (2010) ICNIRP guidelines for limiting exposure to time-varying electric and magnetic fields (1 Hz to 100 kHz) Health Phys 99. https://doi.org/10.1097/HP.0b013e3181f06c86